CHAPTER 9

Computational versus Wind Tunnel Simulation of Atmospheric Boundary Layer Flow for Structural Engineering Applications

DongHun Yeo, M.ASCE*
Liang Shi*

Abstract: *Atmospheric Boundary Layer (ABL) flow simulations have been performed using Large Eddy Simulation (LES) to assess the suitability of the simulated flow for structural wind engineering applications. The governing equations of straight ABL flow for structural engineering purposes were formulated based on state-of-the-art meteorological studies. The balance of the horizontal pressure gradient force and the ground friction was used in the Computational Fluid Dynamics (CFD) solver to achieve dynamic equilibrium throughout the ABL flow. In the simulation using the precursor method, turbulent ABL flow was developed naturally to achieve horizontally homogenous ABL flow. To reduce computational resource requirements this study employed a model scale approach, similar to the approach used in wind tunnel simulations.*

Based on the assessment of the simulated results via comparisons with measurements reported in the literature and values recommended in the ASCE 49-12 Standard for wind tunnel testing, the quality of the simulations for structural engineering applications was found to be comparable with the quality of their wind tunnel counterparts. The results also identified issues, mainly due to grid resolution and inaccurate SGS modeling, that need to be addressed by future research.

Keywords: *Atmospheric boundary layer (ABL); Large eddy simulation (LES); Model scale simulation; Standards; Structural engineering; Turbulence; Wind tunnel testing.*

*Engineering Laboratory, National Institute of Standards and Technology, Gaithersburg, MD 20899, USA (corresponding author), Tel: 1-301-975-8103, Fax: 1-301-869-6275, email: donghun.yeo@nist.gov

1 INTRODUCTION

Wind loads on structures can be determined by using analytical, experimental, and/or numerical simulation approaches. The analytical approach typically specified in codes and standards is widely used in engineering practice. For special structures, however, ad-hoc wind tunnel tests are generally used. Given the cost, turnover times, and reliability issues inherent in wind tunnel testing at the typically small scales required in practice on the one hand, and the rapid development of Computational Fluid Dynamics (CFD) techniques on the other, CFD is increasingly being regarded as a potentially viable simulation option for structural engineering applications. Structural engineers have expressed strong interest in the possibility of using this option, at least for preliminary designs. The UK Design Manual for Roads and Bridges (BD 49/01, HE 2001), the Eurocode (prEN 1991-1-4, CEN 2005), and the Architectural Institute of Japan guidebook (AIJ 2017) allow the use of proven CFD procedures to provide additional design guidance.

With a view to advancing the prospects of using CFD techniques for structural engineering purposes, the National Institute of Standards and Technology (NIST) is engaged in an effort aimed to develop CFD algorithms as a substitute for wind tunnel testing. In this paper we report results achieved within the framework of this effort in the Large Eddy Simulation (LES) of Atmospheric Boundary Layer (ABL) flow. For the simulations to be compatible with currently available computational resources, they need to be performed at scales comparable to those used in wind tunnel simulations. Since the latter are achieved by using empirical devices such as roughness elements, spires, and castellated walls, it was hypothesized that CFD simulations would perform at least as well as their wind tunnel counterparts.

Three approaches have been used to generate neutrally stratified ABL flows in LES studies for wind/structural engineering applications: synthetic turbulence approach, recycling and rescaling approach, and precursor database approach. For reviews of these approaches see Tabor and Baba-Ahmadi (2010), Wu (2017), and Vasaturo et al. (2018).

The synthetic turbulence approach generates at the inflow boundary artificially synthesized wind fluctuations based on target flow characteristics and a predefined mean wind velocity profile (Hémon and Santi 2007, Huang et al. 2010, Kondo et al. 1997, Xie and Castro 2008). This method is computationally efficient and makes it easy to deal with any target characteristics. However, synthetic turbulence structures are less accurate and dissipate faster within the computational domain than naturally developed ones.

The recycling and rescaling method usually prescribes a time-averaged wind velocity profile on the inflow boundary, rescales wind fluctuations collected on a downstream plane, and reintroduces them to the inflow boundary (Kataoka and Mizuno 2002, Nozawa and Tamura 2001). This method has been used for spatially

evolving boundary-layer flows with a zero-pressure gradient, thus reproducing the generation of boundary layer flow in conventional wind tunnel testing facilities, as opposed to the generation of neutrally stratified, horizontally homogeneous ABL flow that, owing to the action of a horizontal pressure gradient, maintains a constant boundary layer height.

The precursor database method generates turbulence in the computational domain by embedding the flow driving mechanism into the cyclic domain without rescaling to achieve fully developed turbulent equilibrium flow (Berthaut-Gerentès et al. 2014, Churchfield et al. 2010; Munters et al. 2016). This precursor method produces a database in auxiliary simulations or in the upstream domain of the main simulation. It entails additional computational costs, but simulates turbulence of the equilibrium ABL flow more realistically than the synthetic turbulence generating methods.

Since straight ABL flow is driven by the balance of horizontal pressure gradient, Coriolis, and ground friction forces, the underlying dynamic equilibrium of the ABL flow can be more accurately achieved by "balanced-force-driven" simulations (Cai et al. 2014, Porté-Agel et al. 2000), rather than by the widely used "boundary-driven" simulations (Aboshosha et al. 2015, Blocken et al. 2007, Huang et al. 2010, Kataoka and Mizuno 2002, Richards and Hoxey 1993, Tominaga 2015).

The simulations considered in this study employed the precursor database method as applied to a neutral balance-force driven ABL. The aim of this paper is to assess the quality of the ABL flow simulated by this technique and compare it to quality of ABL-like flows achieved by conventional boundary-layer wind tunnels techniques as described in standard provisions on the wind tunnel testing procedure.

In this paper, we first describe the numerical simulation of the governing equations of ABL flow, including simulation details. We then present simulation results on the ABL flow characteristics of interest of structural engineering and compare those results with reference data from the literature and standard provisions. ABL simulation features are then discussed, and a flow assessment is presented. The paper ends with concluding remarks.

2 NUMERICAL SIMULATION

2.1 Governing equations of ABL flow

Governing equations for incompressible, neutrally stratified ABL flow are the continuity equation and the momentum equations for Newtonian fluid (i.e., fluid with constant density ρ and kinematic viscosity ν) (e.g., Stull 1988):

$$\nabla \cdot \mathbf{U} = 0 \tag{1}$$

$$\frac{\partial U}{\partial t} + \mathbf{U}\cdot\nabla U + \frac{1}{\rho}\frac{\partial p}{\partial x} - \nu\nabla^2 U + S_x - fV + f^* W \mp V\frac{|\mathbf{U}|}{r} = 0 \quad (2)$$

$$\frac{\partial V}{\partial t} + \mathbf{U}\cdot\nabla V + \frac{1}{\rho}\frac{\partial p}{\partial y} - \nu\nabla^2 V + S_y + fU \pm U\frac{|\mathbf{U}|}{r} = 0 \quad (3)$$

$$\frac{\partial W}{\partial t} + \mathbf{U}\cdot\nabla W + \frac{1}{\rho}\frac{\partial p}{\partial z} - \nu\nabla^2 W + S_z - f^* U = 0 \quad (4)$$

I II III IV V VI VII VIII

where the velocity vector **U** consist of two horizontal velocity components of (U, V) in the (streamwise) x and (lateral) y directions and one vertical component of (W) in the (upward positive) z direction. Term I is the temporal acceleration of the wind flow, Term II expresses the nonlinear interaction of convective accelerations of the flow, Term III expresses the pressure forces induced by the flow (p is the pressure), Term IV expresses the effects of molecular viscosity, Term V represents the source terms (S_x and S_y are the external horizontal pressure gradient forces in the x and y directions; S_z is the body force due to gravity so that $S_z = -g$, where g is the gravity acceleration, Terms VI and VII represent the horizontal and vertical Coriolis forces due to the Earth's rotation (f and f^* are the horizontal and vertical Coriolis force parameters, respectively), and Term VIII denotes the centrifugal force in non-straight winds (r is the radius of curvature of air trajectory).

According to recent studies (Hess 2004, Zilitinkevich 2012, Zilitinkevich et al. 2007, Zilitinkevich and Esau 2002) summarized for structural engineering purposes in Simiu et al. (2016), the contribution of the wind velocity component normal to the surface stress to the resultant mean wind speed is negligible at mid-latitudes. For example, at elevations of the order of, say, 1 km or less, the veering angle is of the order of 5 degrees or less. Thus, Terms VI and VII are not considered in this study. Term VIII is not taken into account because this study only considers the case of non-rotating flows.

This study also assumes that (i) the wind velocity is parallel to the x direction, (ii) the air density is constant throughout the flow, and (iii) the flow is barotropic, that is, the horizontal pressure gradient force is independent of height. Thus, the steady state equilibrium of the fully developed ABL flow can be reached by the external horizontal pressure gradient force (S_x) as a driving force and the friction force on the ground as a retarding force. Thus, the wall-shear stress at the ground is

$$\tau_w = -\frac{\partial p_h}{\partial x} H \quad (5)$$

where H is the height of the computational domain and $\partial p_h/\partial x$ is the external horizontal pressure gradient. Since $\tau_w = \rho u_*^2$ where u_* is the friction velocity, it

follows from Eq. (5) and the logarithmic law describing the dependence of the mean wind speed with height that:

$$\frac{\partial p_h}{\partial x} = -\frac{\rho}{H} u_*^2 = -\frac{\rho}{H}\left[\frac{\kappa U(z_{\text{ref}})}{ln(z_{\text{ref}}/z_0)}\right]^2 \tag{6}$$

where $U(z_{\text{ref}})$ is the longitudinal wind velocity at height z_{ref}, z_0 is the surface roughness length, and $\kappa = 0.41$ is the von Kármán constant.

Therefore, Eqs. (2) through Eq. (4) become

$$\frac{\partial U}{\partial t} + \mathbf{U}\cdot\nabla U + \frac{1}{\rho}\frac{\partial p}{\partial x} - \nu\nabla^2 U + \frac{1}{\rho}\frac{\partial p_h}{\partial x} = 0 \tag{7}$$

$$\frac{\partial V}{\partial t} + \mathbf{U}\cdot\nabla V + \frac{1}{\rho}\frac{\partial p}{\partial y} - \nu\nabla^2 V = 0 \tag{8}$$

$$\frac{\partial W}{\partial t} + \mathbf{U}\cdot\nabla W + \frac{1}{\rho}\frac{\partial p}{\partial z} - \nu\nabla^2 W + g = 0. \tag{9}$$

2.2 Large-Eddy Simulation

Through a spatial low-pass filter based on the scale of grid spacing, Eqs. (7) through Eq. (9) can be converted to the filtered equations for LES:

$$\nabla\cdot\tilde{\mathbf{U}} = 0 \tag{10}$$

$$\frac{\partial\tilde{\mathbf{U}}}{\partial t} + \tilde{\mathbf{U}}\cdot\nabla\tilde{\mathbf{U}} + \frac{1}{\rho}\nabla\tilde{P} - \nu\nabla^2\tilde{\mathbf{U}} + \nabla\cdot\boldsymbol{\tau}^{\mathbf{d}} + \mathbf{F} = 0 \tag{11}$$

where the filtered quantity is denoted by a tilde, P consists of pressure p and the isotropic component of the subgrid-scale (SGS) stress $\boldsymbol{\tau}$, $\boldsymbol{\tau}^{\mathbf{d}}$ is the deviatoric component of the SGS stress, and $\mathbf{F}$ is the external body force [i.e., $-(1/\rho)\partial p_h/\partial x$ in the x direction and $-g$ in the z directions, as shown in Eqs. (7) and (9) respectively]. To close the LES equations, a model for the SGS stress tensor $\boldsymbol{\tau}$ is required, to simulate the energy transfer between resolved motions and SGS modeled motions.

2.3 Simulation details

All the simulations were performed using LES with the one-equation turbulent energy SGS model (Yoshizawa and Horiuti 1985) in OpenFOAM v. 2.4.0 (2015). In this study it was assumed that the pressure gradient and temperature do not vary

with height. The model length scale was 1:1000 as in wind tunnel tests for high-rise buildings (e.g., Tanaka et al. 2013). The terrain exposure was assumed to be open (roughness length $z_0 = 0.03$m at full scale, ASCE 2010). The target mean along-wind speed at the top was set to $\overline{U}(H) = 10$ m/s. The surface friction velocity was calculated from the logarithmic velocity profile $u_* = \kappa \overline{U}(H)/ln(H/z_0) = 0.394$ m/s. The wall-shear stress on the ground and the horizontal pressure gradient were determined from the balance of forces [Eqs. (5) and (6)], respectively. The kinematic viscosity of air was assumed to be $\nu = 1.455 \times 10^{-5}$ m^2/s.

As shown in Figure 1, the dimensions of the computational domain were $L{:}W{:}H = 2{:}1{:}1$ where $H = 1$ m. The grid was uniform ($\Delta/H = 0.01$) in all directions, and the total number of cells was 2×10^6 (200, 100 and 100 cells in the x, y, and z direction, respectively). The non-dimensional time step Δt^* (defined as $\Delta t^* = U(H)\Delta t/H$) was 0.0025, and the total non-dimensional time for analysis was approximately 200.

Periodic boundary conditions were employed in all horizontal directions so that the ABL flow is fully developed regardless of the along-wind dimension of the domain. The slip wall condition was imposed on the top boundary for velocity (i.e., zero normal velocity and zero gradient tangential velocity). The zero-gradient boundary condition was applied to the ground and top boundaries for pressure. The wall-shear model (Schumann 1975) was employed at the center of the first grid above the ground (denoted by subscript $\Delta 1$) in the xz and yz directions to achieve local equilibrium in the near wall-region:

$$\begin{aligned}
\tau_{xz,\mathrm{wall}}(x_{\Delta 1}, y_{\Delta 1}, t) &= -\rho u_*^2 \frac{U_{\Delta 1}(x_{\Delta 1}, y_{\Delta 1}, t)}{|\mathbf{U}_{\Delta 1}|} \\
&= -\rho \left[\frac{\kappa |\mathbf{U}_{\Delta 1}|}{\mathrm{In}(z_{\Delta 1}/z_0)}\right]^2 \frac{U_{\Delta 1}(x_{\Delta 1}, y_{\Delta 1}, t)}{|\mathbf{U}_{\Delta 1}|} \\
\tau_{yz,\mathrm{wall}}(x_{\Delta 1}, y_{\Delta 1}, t) &= -\rho u_*^2 \frac{V_{\Delta 1}(x_{\Delta 1}, y_{\Delta 1}, t)}{|\mathbf{U}_{\Delta 1}|} \\
&= -\rho \left[\frac{\kappa |\mathbf{U}_{\Delta 1}|}{\mathrm{In}(z_{\Delta 1}/z_0)}\right]^2 \frac{V_{\Delta 1}(x_{\Delta 1}, y_{\Delta 1}, t)}{|\mathbf{U}_{\Delta 1}|}
\end{aligned} \tag{12}$$

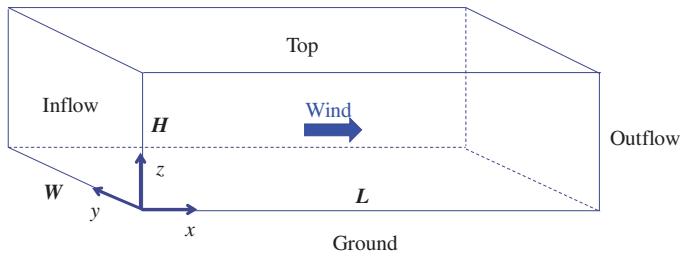

Figure 1. Computational domain of simulation

where $|\mathbf{U}_{\Delta 1}|$ is the spatial average of $\mathbf{U}$ on the xy-plane at the height of $z_{\Delta 1}$. The friction velocity in this model was obtained from the horizontally averaged velocity at each time step by assuming a logarithmic mean profile near the ground (Grötzbach 1987) instead of a fixed value from the momentum balance in the original Schumann model. The initial conditions for the velocity consist not only of the target logarithmic along-wind wind velocity in the domain but also of small perturbations near the ground, which expedite the development of the turbulence in the simulations. Details of this model-scale ABL simulation are provided in Shi and Yeo (2016, 2017).

3 CHARACTERISTICS OF SIMULATED ABL FLOWS

The characteristics of the simulated ABL flow assumed in this study for structural engineering applications are compared with their counterparts in the literature and the ASCE 49-12 Standard for wind tunnel (ASCE 2012).

The simulated ABL wind velocities (U, V, W) were decomposed into mean velocities ($\overline{U},\overline{V},\overline{W}$) and wind velocity fluctuations (u, v, w) along the x-, y-, and z-axes, respectively, corresponding to the streamwise, lateral, and vertical directions:

$$U(z,t)=\overline{U}(z)+u(z,t), V(z,t)=\overline{V}(z)+v(z,t), W(z,t)=\overline{W}(z)+w(z,t). \quad (13)$$

The following subsections examine the characteristics of the mean velocities and fluctuating components of the simulated flow.

3.1 Mean wind speed profile

The ABL flow was assumed to follow the logarithmic law:

$$\overline{U}(z)=\frac{u_*}{\kappa}\mathrm{In}\left(\frac{z}{z_0}\right). \quad (14)$$

Figure 2 shows the mean streamwise velocity profile of the simulated flow at $x/H=1$ and $y/H=0.5$ and the logarithmic law fit to the velocity data. The friction velocity u_* and the reference mean wind speed $\overline{U}(H)$ in Eq. (14) were estimated from the simulation result to be 0.438 m/s and 11.124 m/s, respectively, which are higher than the target values of 0.394 m/s and 10 m/s. The differences could be ascribed to the well-known log-layer mismatch due to the inaccuracy of the SGS model near the ground in the LES simulation (Mason and Thomson 1992). The simulated values are employed hereinafter for normalizing the flow characteristics.

The ASCE 49-12 Standard specifies the wind speed profile of the incoming ABL flow for the use of wind tunnel testing as

$$\overline{U}_{ASCE49}(z)=\overline{U}(z_{ref})\left(\frac{z}{z_{ref}}\right)^{\overline{\alpha}} \quad (15)$$

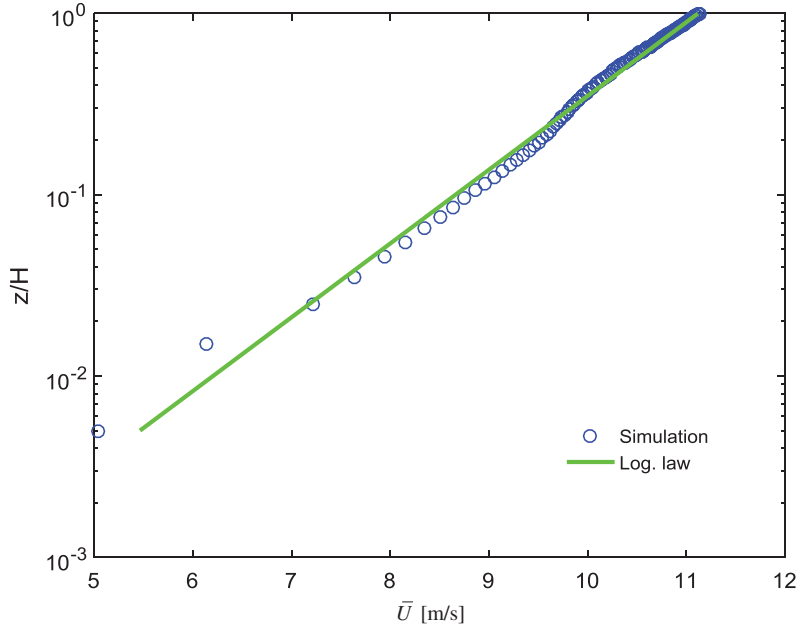

Figure 2. Logarithmic fit to mean streamwise velocity profile

where $\overline{\alpha} = 0.14$ for the open terrain exposure. ASCE 49-12 states that the mean wind speed power law exponent shall be within ±15% of the target value. Because the gradient height provision ($z_g = 274$ m in open terrain exposure) in the standard is not consistent with the state-of-the-art ABL flow description in the meteorological literature (see, e.g., Simiu et al. 2016 for a summary and an application to high-rise building design), the gradient height is not considered in the plot of the wind speed profile.

Figure 3 shows the mean wind speed profile as simulated in this study, the target logarithmic law profile, and the profiles accepted by ASCE 49-12. The simulation results in differences with respect to the logarithmic profile up to 5% near the ground (i.e., $z/H < 0.02$) and less than 2% at the other elevations. Those differences are well within the accepted range considered by the ASCE 49-12 Standard to be acceptable and are lower than those typical of wind tunnel tests (Kozmar 2011, Samali et al. 2004).

3.2 Turbulence intensity

The turbulence intensity at a point with height z is defined as the ratio of the root-mean-square of the velocity fluctuations to the longitudinal mean wind speed at that height:

$$I_u(z) = \frac{\sqrt{\overline{u^2(z)}}}{\overline{U}(z_{ref})}, \quad I_v(z) = \frac{\sqrt{\overline{v^2(z)}}}{\overline{U}(z_{ref})}, \quad I_w(z) = \frac{\sqrt{\overline{w^2(z)}}}{\overline{U}(z_{ref})} \tag{16}$$

where in this study z_{ref} is the ABL height H.

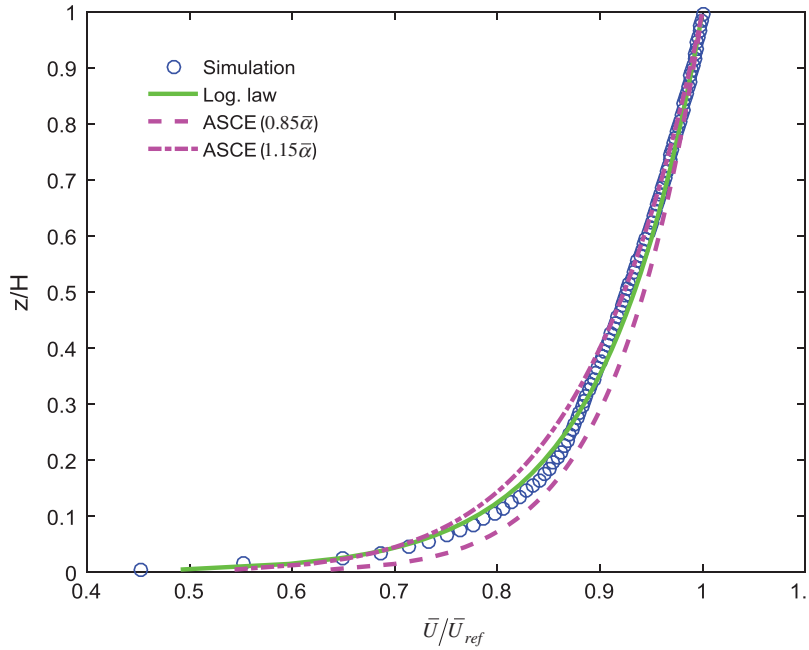

Figure 3. Mean streamwise velocity profiles

Turbulence intensities over open terrain exposure in the Atmospheric Surface Layer (ASL) e.g., $z/H \lesssim 0.1$) are, according to ASCE 49-12

$$I_u(z) = \frac{1}{\ln(z/z_0)}, \quad I_v(z) = \frac{0.8}{\ln(z/z_0)}, \quad I_w(z) = \frac{0.5}{\ln(z/z_0)} \tag{17}$$

The turbulence intensity profiles in the neutral ABL flow suggested by Stull (1988) are

$$\begin{aligned} I_u(z) &= u_* \left[6\left(1 - \frac{z}{H}\right)^2 + \frac{\overline{u^2(H)}}{u_*^2} \frac{z}{z_H} \right]^{1/2} / U(z) \\ I_v(z) &= u_* \left[3\left(1 - \frac{z}{H}\right)^2 + \frac{\overline{v^2(H)}}{u_*^2} \frac{z}{z_H} \right]^{1/2} / U(z) \\ I_w(z) &= u_* \left(1 - \frac{z}{H}\right)^{1/4} / U(z). \end{aligned} \tag{18}$$

Figure 4 presents the turbulence intensities determined from Eqs. (17) and (18) and obtained in the simulations. For $0.03 \le z/H \le 0.8$, the simulation yields I_u values that deviate from target values by approximately −5% to 10%, I_w values

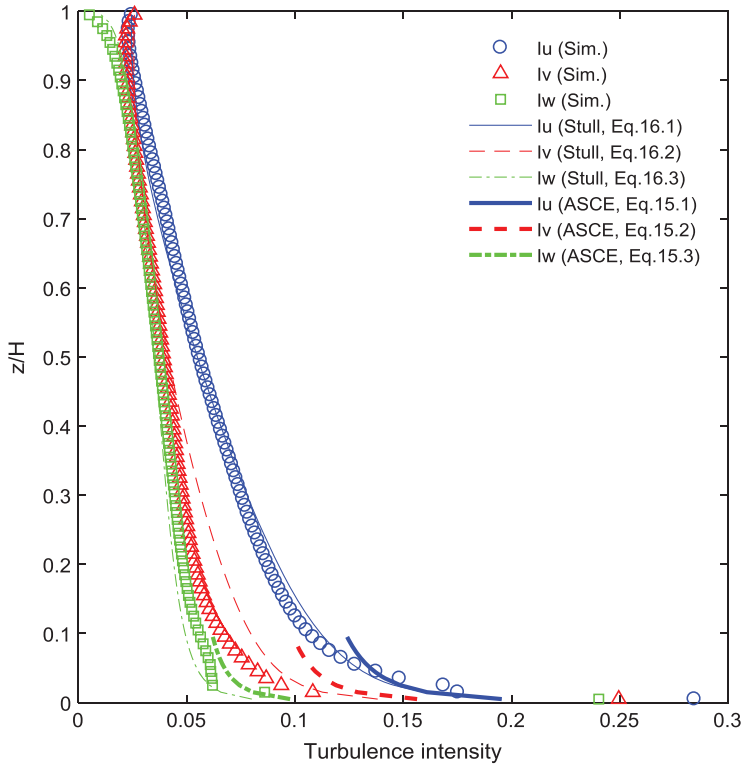

Figure 4. Turbulence intensities

that exceed target values by less than 14%, and I_v values that are smaller than target values by less than 20%, where the target values are given by Eq. (18). The turbulence intensity simulations in the study outperform their counterparts simulated in typical wind tunnel tests (Kozmar 2011, Samali et al. 2004, Tanaka et al. 2013).

The ratios of the three turbulence intensities $(I_v/I_u, I_w/I_u)$ in the lower ABL are shown in Figure 5. The ratios from the simulations are 0.62:0.53 for $0.07 < z/H < 0.2$, which are comparable with the ratios of 0.7:0.45 from Stull (Eq. 18), 0.75~0.8:0.5 from ASCE 49-12 (Eq. 17), 0.5~0.6:0.3~0.4 from Counihan (1975), and 0.78~0.82:0.55~0.63 from ESDU 85020 (2001). Note that the ratio I_v/I_u is smaller by 14% than its counterpart suggested by Stull because the turbulence intensity in the lateral direction (I_v) is relatively low in the simulations.

3.3 Wind velocity spectra

The spectral density functions of wind velocity fluctuations are a measure of the contribution of each frequency component of the fluctuations to the variance of the fluctuations. Among several proposed spectral density functions for wind engineering purpose, useful non-dimensional spectra for the longitudinal, lateral,

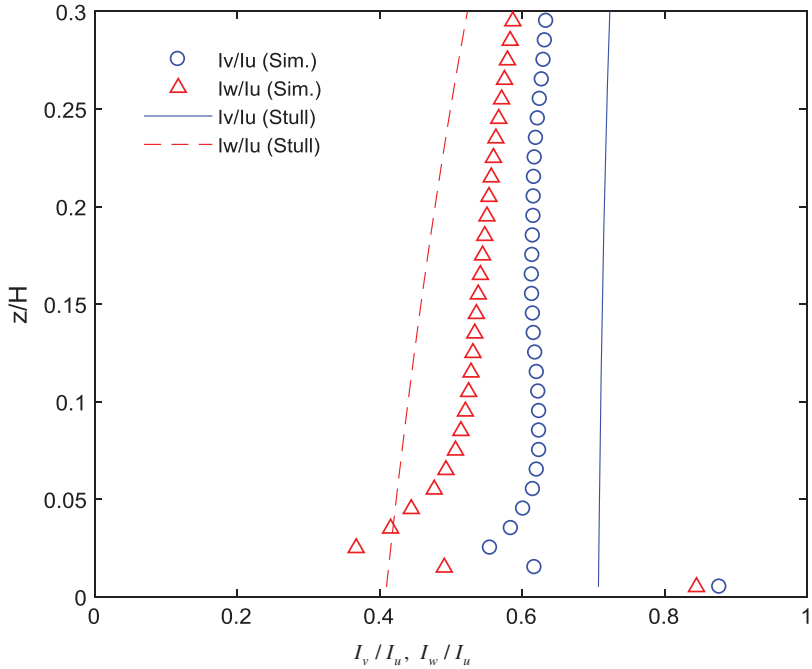

Figure 5. Ratios of turbulence intensities

and vertical turbulence at elevation z are expressed respectively as (Kaimal et al. 1972, Simiu 2011)

$$\frac{nS_u(z,n)}{u_*^2} = \frac{200f}{(1+50f)^{5/3}}, \quad \frac{nS_v(z,n)}{u_*^2} = \frac{15f}{(1+10f)^{5/3}}, \quad \frac{nS_w(z,n)}{u_*^2} = \frac{3.36f}{1+10f^{5/3}} \tag{19}$$

where f is the Monin coordinate defined as $f = nz/\overline{U}(z)$ where n is the frequency of wind velocity fluctuations. Equation (19, Part 1) differs slightly from its Kaimal et al. (1972) counterpart in that it corresponds to a mean square value of the turbulence fluctuations equal to $6u_*^2$, a value widely accepted for wind engineering purposes (Simiu and Scanlan 1996).

Figure 6 shows the non-dimensional spectra at $z/H = 0.1$. The resolved fluctuations in LES follow Eq. (19) in the inertial subrange (the slope of $-2/3$ in the plot). Note that the lower limit of the inertial subrange is on the order of $f \approx 0.1 - 0.2$ (Busch and Panofsky 1968, Drobinski et al. 2004, Fichtl and McVehil 1970, Singer et al. 1968). The deficit is also observed in the simulated flow of low-frequency and high-frequency components.

The low-frequency spectrum deficit problem is related to the size of the computational domain and the length of simulation time (Nozawa and Tamura 2001). This is experienced not only in CFD simulations but also in wind tunnel

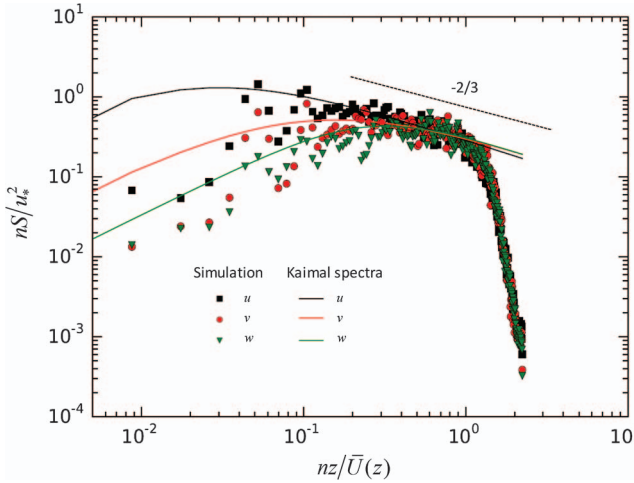

Figure 6. Spectra of wind velocity components at z/H = 0.1
Source: Shi and Yeo (2017).

testing (Simiu et al. 2011). The missing low-frequency components have little or no influence on the signature turbulence of structures immersed in the ABL flow but produce quasi-static effects on the response to the structures. The contribution of low-frequency component to the peak structural response can therefore be taken into account via post-processing (Asghari Mooneghi et al. 2016, Yeo and Chowdhury 2013). This approach can be applied not only to wind tunnel simulations, but to CFD simulations as well.

The high-frequency spectrum deficit problem is mainly caused by insufficient grid resolution and inaccurate SGS modeling of LES. LES resolves large-scale fluctuations up to a frequency related to grid scales, $f \approx 2.5$ (Figure 6). As shown in Figure 6, the resolved eddies follow the target spectra up to $f \approx 1$ and deviate from them for $f > 1$. This deviation is mainly caused by performance of the imperfect SGS modeling (e.g., by excessive SGS dissipation that moves too much energy from the resolved motions to the SGS motions). Such SGS modeling causes the logarithmic layer mismatch (LLM) near the ground, which generates "overshoot" peak wind shear, oversized streamwise coherence and, ultimately, inaccurate prediction of wind velocity field near the ground (Brasseur and Wei 2010, Mason and Thomson 1992, Yang et al. 2017). However, Because the overshoot occurs close to the ground, its effect is typically modest from a structural engineering point of view and is negligible for tall building design.

3.4 Wind velocity cross-spectra

The cross-spectral density functions of the wind velocity fluctuations at two different points are measures of the coherence of harmonic fluctuating components with frequencies n at those points. Since the cross-spectral density function is a function of the co-spectrum and the quadrature spectrum is negligible in

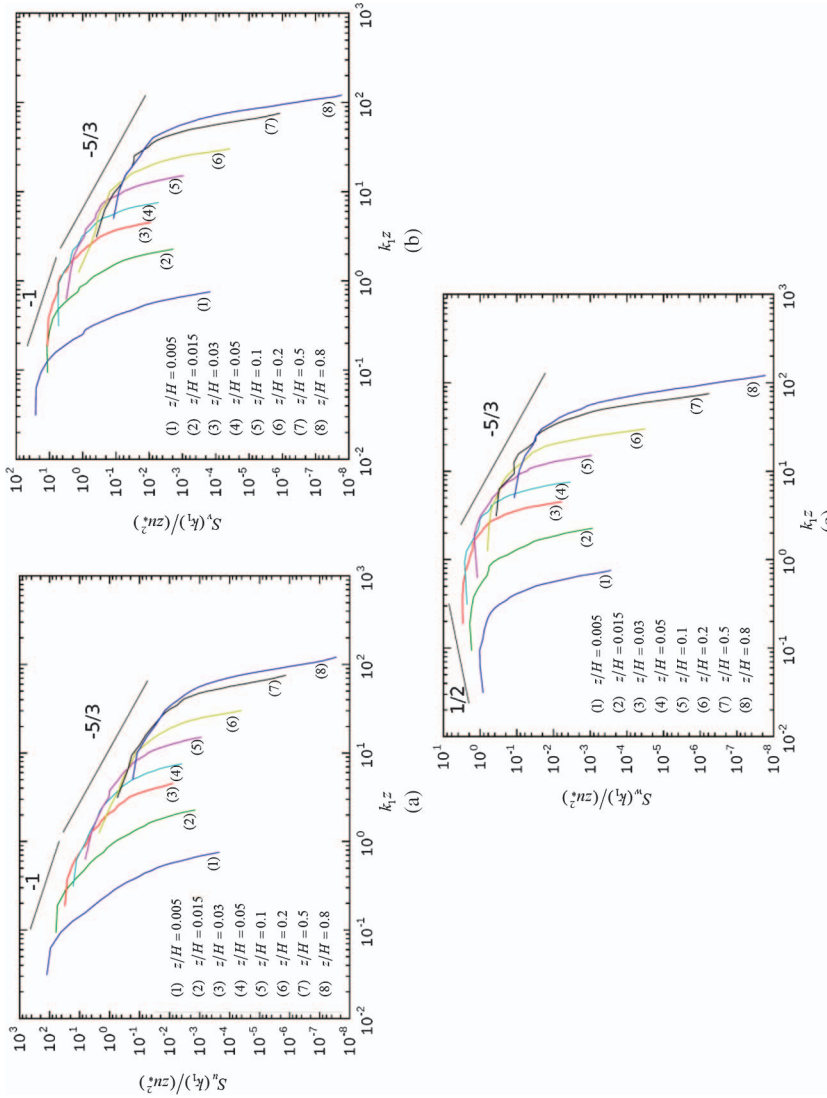

Figure 7. Spatial spectra of wind velocity components over elevations: (a) $S_u(k_1)$, (b) $S_v(k_1)$, and (c) $S_W(k_1)$

homogeneous turbulent ABL flows (Teunissen 1970), the co-spectrum can be expressed as (Simiu and Scanlan 1996)

$$S_{ii}^{c}(y_1, z_1; y_2, z_2; n) = S_i^{1/2}(z_1, n) S_i^{1/2}(z_2, n) e^{-\hat{f}} \tag{20}$$

where (y_1, z_1) and (y_2, z_2) denotes the coordinates in the lateral and vertical directions of two different points in a plane normal to the wind direction, the subscript i stands for the u, v, and w components, and $e^{-\hat{f}}$ describes the coherence of velocity components at those points. The expression for the exponent $\hat{f}$ proposed by Davenport (1968) is

$$\hat{f} = \frac{n[C_z^2(z_1 - z_2)^2 + C_y^2(y_1 - y_2)^2]^{1/2}}{\frac{1}{2}[U(z_1) + U(z_2)]} \tag{21}$$

where C_z and C_y are exponential decay coefficient. Their values differ considerably from study to study (Simiu and Scanlan 1996). Commonly accepted values for the decay coefficients are $C_z = 10$, $C_y = 16$ (Vickery 1970). A similar expression was proposed for the exponential decay function in the x direction with a suggested exponential decay coefficient $C_x = 3$ to 6 (see, e.g., Simiu and Scanlan 1996).

Figure 8 shows the coherence functions $e^{-\hat{f}}$ for $u(t)$ at two locations along the directions x, y, and z. The mean streamwise velocity $\overline{U}(z)$ for C_z is the average of the mean velocities at two locations, as shown in Eq. (21). The estimated exponential decay coefficients of the simulated flow: $C_x = 1.00 \pm 0.03$, $C_y = 14.1 \pm 0.4$, and $C_z = 11.5 \pm 0.4$, where the sign $\pm$ denotes the standard deviation with respect to the fitted curve. The coefficients of C_y and C_z in the simulations are in agreement to within 15% from the suggested values. However, C_x from the simulation is lower by a factor of at least 3 than the suggested value, which implies that the simulation produces significantly larger streamwise turbulence eddies at $z/H = 0.1$. This could be explained by the LLM problem in LES, which leads to excessive streamwise coherence near the ground.

3.5 Integral length scales

The integral length scales of turbulence are a measure of the representative size of the energy-bearing eddies in the flow and consist of nine components corresponding to the three dimensions (i.e., x, y, and z) of eddies associated with the three velocity fluctuation components. For example, L_u^x, L_u^y, and, L_u^z are the characteristic eddy sizes in the x, y, and z directions, respectively, associated with the longitudinal wind velocity fluctuations u. The length scale of L_u^x, which is the most common measure in wind engineering practice, is defined as (Counihan 1975, Simiu and Scanlan 1996)

$$L_u^x = \frac{1}{\overline{u^2}} \int_0^\infty R_{u_1 u_2}(x) dx \tag{22}$$

where $R_{u_1 u_2}(x)$ is the cross-covariance function of the two longitudinal velocity components at two spatial positions of $u_1 = u(x_1, y_1, z_1, t)$ and

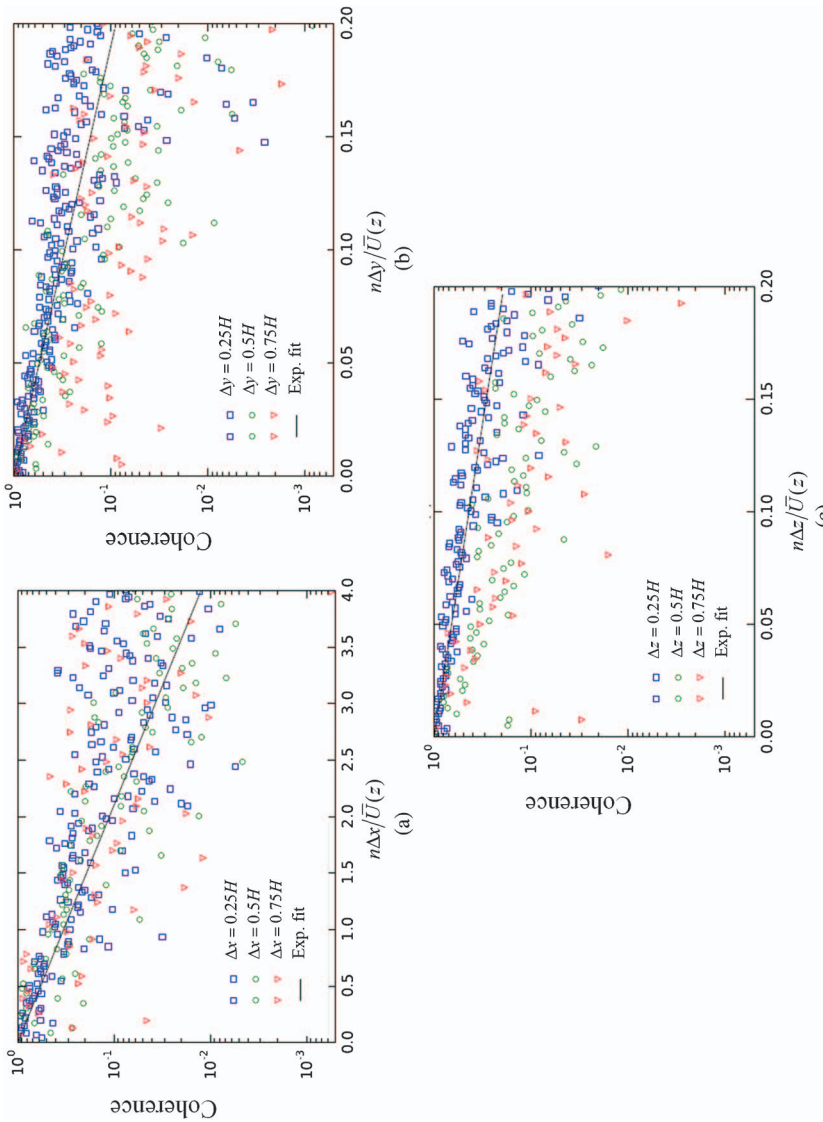

Figure 8. Coherence of wind fluctuations u(t): (a) x direction, (b) y direction, and (c) z direction
Source: Plot (a) from Shi and Yeo 2017).

$u_2 = u(x_1 + x, y_1, z_1, t)$. Alternatively, the length scale can be estimated based on the Taylor's hypothesis of frozen turbulence as follows (Simiu and Scanlan 1996):

$$L_u^x = \frac{U}{\overline{u^2}} \int_0^\infty R_u(\tau) d\tau \tag{23}$$

where $R_u(\tau)$ is the auto-covariance function of the fluctuation $u(t)$ at time lag τ.

The integral length scale L_u^x within the ASL increases with height and decreases over rougher surface terrain (Counihan 1975). The reported values of L_u^x have large variability (ASCE 2012, Simiu and Scanlan 1996). An estimate of L_u^x within the ASL reported in ASCE 49-12 is expressed as

$$L_u^x = \frac{z}{2\pi f_m} \tag{24}$$

where f_m is the Monin reduced frequency at which the spectrum $nS(u)/u_*^2$ reaches the maximum value. The typical value suggested in ASCE 49-12 is $f_m \approx 0.032$, although no validation for this value appears to be available in the literature, which is lower than the counterpart in the simulation ($f_m \approx 0.05$ at $z/H = 0.1$ in Figure 6). However, Pasquill and Butler (1964) state that Eq. (24) can result in the underestimation of L_u^x by a factor of 2 to 3.

An alternative approximate expression of L_u^x was proposed by Counihan (1975):

$$L_u^x \approx Cz^m \quad (L_u^x \text{ and } z \text{ in meters}) \tag{25}$$

where the constant C and m are determined using Figure 13 of Counihan (1975). The proposed estimates L_u^y and L_u^z are

$$L_u^y \approx 0.35 L_u^x, \quad L_u^z \approx 0.5 L_u^x. \tag{26}$$

Figure 9 shows the integral scales of streamwise wind fluctuations in the x, y, and z directions. The symbols represent simulation results in this study. The curves show Counihan's estimates [Eqs. (25) and (26)]. For $z/H = 0.1$, the estimate of L_u^x/H in ASCE 49-12 [Eq. (24)] is 0.32. As shown in Figure 9, the simulation results are qualitatively consistent with the inequalities $L_u^x > L_u^z > L_u^y$ in the lower ABL height ($z/H \le 0.3$ in this study). The ratios L_u^x:L_u^y:L_u^z in the simulation are approximately 1:0.25:0.75 for $z/H \le 0.3$, which is comparable to Eq. (26). While the simulated values of L_u^x and L_u^y are in good agreement with Counihan's estimates [Eqs. (25) and (26)], the simulated values of L_u^z at $z/H = 0.2 \sim 0.3$ are larger by a factor of about 2 than the values proposed in the literature. The peaks of the L_u^x and L_u^z profiles occur at $z/H \approx 0.35$ and 0.55, respectively, and decrease above the elevations of the peaks. L_u^y is almost constant throughout the ABL height. In view of the substantial uncertainties in the estimation of the integral turbulence lengths and of the fact that the latter need not be used in engineering calculations—especially if Eq. (19), rather than the von Kármán spectrum, are used for the spectral densities of the velocity fluctuations—such uncertainties are of limited or no practical significance from a structural engineering viewpoint.

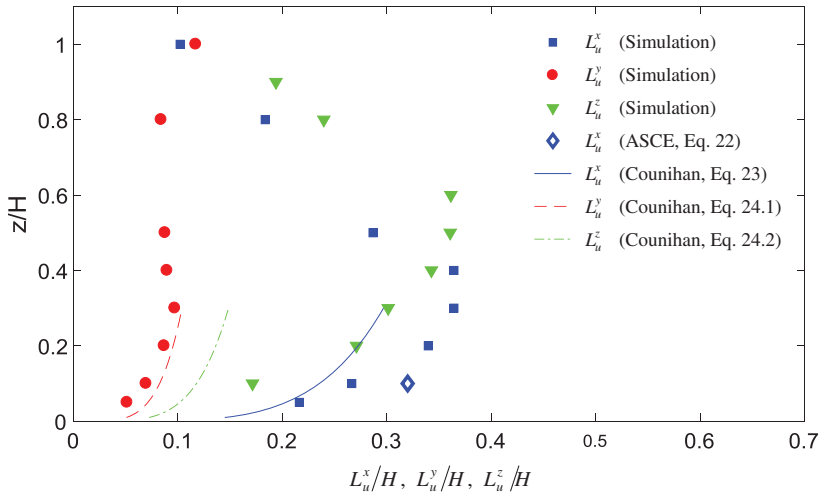

Figure 9. Integral length scales: Numerical simulations
Source: Counihan (1975), ASCE 49-12 (2012).

4 DISCUSSION

4.1 ABL simulation

This LES ABL simulation presented in this paper is based on (i) the use of state-of-the-art ABL research in wind/structural engineering applications, (ii) the balanced-force-driven ABL wind model, (iii) the precursor method, and (iv) a model scale similar to scales used in wind tunnel testing for tall building design applications.

Use of state-of-the-art ABL research in wind/structural engineering applications. Recent meteorological studies in the ABL study show that the ABL wind velocity profile in the mid-latitude region is approximately logarithmic up to elevations of an order of 1 km above the surface and that the veering angle for the elevations is negligible for practical purposes. The state-of-the-art results imply that the governing equations of the ABL flow as used for current structural engineering applications can be simplified by eliminating the Coriolis force terms.

Balanced-force-driven ABL wind model. In CWE applications, ABL simulations typically use "boundary-driven" wind to generate ABL flows by specifying inflow/outflow and top boundary conditions. This approach does not take into account the dynamic equilibrium of the neutrally stratified ABL flow and hence is not optimal for horizontally homogeneous ABL flow simulations. The "balanced-force-driven" approach employs the dynamic equilibrium of the ABL flow using balance of the horizontal pressure gradient force (which drives the wind flow) and the friction force (which retards the wind flow).

Precursor method. The precursor method, in conjunction with the balanced-force-driven mechanism, naturally develops turbulence by shear stress near the

surface, and generates more realistic ABL flows than other methods do. The simulated flow using the precursor method can be stored in databases and be used as incoming flow in a main simulation with objects immersed in the ABL. Though the database of incoming ABL flows from the promising precursor-based simulations requires additional computational time and storage, it allows wind/structural engineering practitioners to perform CFD simulations of ABL flows conveniently and with reduced uncertainties.

The ABL flows simulated by the precursor method are influenced by the periodic boundary condition inherent in the method. The effects of the boundary condition on the simulated flow become weaker as the size of the computational domain increases. Sensitivity studies are recommended to ascertain whether the size of the computational domain is adequate.

Model scale. The LES simulation in this study was performed using scaled length and velocity but employing the viscosity of air, as wind conventional tunnel testing does. One consequence of the reduced model scale—and the consequent violation of the Reynolds number with respect to its prototype counterpart—is that computational costs become affordable for practical wind engineering purposes.

To achieve a ground surface roughness that causes the flow to be independent of viscosity (Isyumov 2014, Sutton 1953), the ASCE 49-12 Standard specifies for the wind-tunnel-scaled flow a surface-roughness Reynolds number $Re_T = u_* z_0/\nu > 2.5$, where Re_T is in effect the ratio of a turbulent eddy viscosity to the molecular viscosity. This approach is not necessary in CWE precursor method computations, which do not model roughness length but rather shear stresses and a sufficient flow-development length.

This paper examined the case of length scales of the order of 1:1000. This scale is comparable to model scales used for the simulation of wind effects on high-rise buildings. The approach considered in this paper can readily be modified to accommodate simulations of low-rise buildings as well. Typical wind tunnel scales for such buildings are of the order of 1:100 for length and 1:5 for velocity. To achieve CWE simulations comparable to wind tunnel simulations the same scales can be adopted for CWE simulations as well.

4.2 Assessment of simulated ABL flow

As shown in the section, Characteristics of Simulated ABL Flows, the quality of the flow simulated in this study satisfies criteria set forth in the ASCE 49-12 Standard for wind tunnel testing.

The mean wind speed profile follows the logarithmic law with differences of less than 2% at most elevations. The turbulence intensities are in good agreement with the standard values (to within 10% for I_u, 14% for I_w, and 20% for I_v). The predicted coherence and the integral length scales of the ABL flow differ from models typically assumed in engineering calculations by amounts that vary from 15% to more than 100%. However, those models are themselves very uncertain, and differ from reported full-scale measured values by ±100% or even more.

The wind velocity spectra are well reproduced in the non-dimensional frequency range $0.05 \leq f \leq 1$. For example, for a building with height $h = 183$ m under

wind speed of $\overline{U}(10\text{ m}) = 35$ m/s, to $f = 1$ there corresponds a frequency 0.29 Hz, well above the first three lowest natural frequencies of vibration of the building, which were determined to be 0.165 Hz, 0.174 Hz and 0.188 Hz (Park and Yeo 2016). These results show that the simulated ABL flow is capable of producing resonant response in the first three modes for the building considered in this example. More generally, the ASCE 7-16 Standard defines rigid buildings (i.e., buildings not susceptible to experiencing resonant response) as buildings with fundamental natural frequencies in excess of 1 Hz; flexible buildings are therefore buildings with frequencies $n \leq 1$ Hz. This can be achieved by using more refined grids or better performed SGS models than those used in this study. Aerodynamic effects of unresolved, small-sized fluctuations are considered in LES by SGS models. For applications in which the simulation of small eddies is important, it is necessary to study the capability of SGS models to produce effects associated with such eddies. This topic should be the object of future research. The effects of missing low-frequency components ($f < 0.05$ in this study) on structural response can be compensated for by using post-processing corrections, as mentioned in Section 3.3.

This study confirms the existence of the well-known logarithmic layer mismatch problem (even worse with buoyancy effects) caused by inaccurate SGS modeling near the ground, where it overestimates the streamwise coherence, a feature that is conservative from a structural engineering viewpoint.

Simulated flow is influenced by the periodic boundary conditions, and the associated along-wind domain length affects coherence of flow. A "wiggled" spectrum in low-frequency component is a consequence of the periodic boundary conditions. As noted by Nozawa and Tamura (2001), this influence is stronger in the upper region of the ABL, owing to the shorter turnover period caused by the higher velocities in that region. Underestimated lateral fluctuations in the y direction are observed as well, which require further investigation.

5 CONCLUDING REMARKS

ABL simulations using LES have been performed to assess the extent to which CWE simulations of ABL flows are comparable to their counterpart conventional wind tunnel simulations. For structural engineering purposes, the governing equations of straight ABL flow were formulated based on state-of-the-art meteorological studies. The balanced forces between horizontal pressure gradient and ground friction were adapted to the CFD solver to achieve dynamic equilibrium throughout ABL. In the simulation using the precursor method, the turbulent ABL flow was naturally developed to achieve horizontally homogenous ABL flow. To reduce computational resource requirements this study employed a model scale approach, similar to the approach used in wind tunnel simulations.

The characteristics of simulated ABL flow were investigated and compared with their counterparts in the literature and the ASCE 49-12 Standard for wind tunnel testing. The mean wind speed profile accurately followed the logarithmic

law to within 2% differences at most elevations. The turbulence intensities were found to be in good agreement with standard values, to within 10% for I_u, 14% for I_w, and 20% for I_v. The wind velocity spectra were correctly simulated in the inertial subrange. The coherence and the integral length scales of the ABL flow were adequately predicted, with differences with respect to models proposed in the literature comparable to differences among most reported prototype measurements. The results also identified issues, mainly due to inaccurate SGS modeling, that need to be addressed in future research. The main conclusion of this study is that LES simulations of the lower 1 km of the turbulent, neutrally stratified ABL can be produced that achieve a level of quality equal to or higher than state-of-the-art, conventional boundary-layer wind tunnel simulations.

This paper examined the case of length scales of the order of 1:1000. This scale is comparable to model scales used for the simulation of wind effects on high-rise buildings. The approach considered in this paper can readily be modified to accommodate simulations of low-rise buildings as well. Typical wind tunnel scales for such buildings are of the order of 1:100 for length and 1:5 for velocity. To achieve CWE simulations comparable to wind tunnel simulations the same scales can be adopted for CWE simulations as well.

Based on the assessment of the simulated results via comparisons with measurements reported in the literature and values recommended in the ASCE 49-12 Standard for wind tunnel testing, the quality of the simulations for structural engineering applications was found to be comparable with the quality of their wind tunnel counterparts. The results also identified issues, mainly due to grid resolution and inaccurate SGS modeling, that need to be addressed by future research.

ACKNOWLEDGMENTS

The authors are indebted to Dr. Tarak Nandi for providing useful inputs regarding estimation of the turbulence intensities and integral length scales of the simulated flow. The contributions to this paper by Dr. Emil Simiu, who served as project leader, are acknowledged with thanks.

References

Aboshosha, H., A. Elshaer, G. T. Bitsuamlak, and A. El Damatty. 2015. "Consistent inflow turbulence generator for LES evaluation of wind-induced responses for tall buildings." *J. Wind Eng. Ind. Aerodyn.* **142**: 198–216.

AIJ (Architectural Institute of Japan). 2017. *Guidebook of recommendation for loads on buildings 2: Wind-induced response and load estimation/Practical guides of CFD for wind resistant design*. Tokyo: AIJ.

ASCE. 2010. *Minimum design loads for buildings and other structures*. ASCE/SEI 7-10. Reston, VA: ASCE.

ASCE. 2012. *Wind tunnel testing for buildings and other structures*. ASCE/SEI 49-12. Reston, VA: ASCE.

Asghari Mooneghi, M., P. A. Irwin, and A. Gan Chowdhury. 2016. "Partial turbulence simulation method for predicting peak wind loads on small structures and building appurtenances." *J. Wind Eng. Ind. Aerodyn.* **157**: 47–62.

Berthaut-Gerentès, J., D. Delaunay, and S. Sanquer. 2014 "Atmospheric turbulent layer simulation providing unsteady inlet conditions for large eddy simulation." In *6th Int. Symp. on Computational Wind Engineering (CWE 2014)*. Hamburg, Germany.

Blocken, B., T. Stathopoulos, and J. Carmeliet. 2007. "CFD simulation of the atmospheric boundary layer: Wall function problems." *Atmos. Environ.* **41** (2): 238–252.

Brasseur, J. G., and T. Wei. 2010. "Designing large-eddy simulation of the turbulent boundary layer to capture law-of-the-wall scaling." *Phys. Fluids* **22** (2): 021303.

Busch, N. E., and H. A. Panofsky. 1968. "Recent spectra of atmospheric turbulence." *Q. J. R. Meteorol. Soc.* **94** (400): 132–148.

Cai, X., Q. Huo, L. Kang, and Y. Song. 2014. "Equilibrium atmospheric boundary-layer flow: Computational fluid dynamics simulation with balanced forces." *Boundary Layer Meteorol.* **152** (3): 349–366.

CEN (European Committee for Standardization). 2005. *Actions on structures. Part 1-4: Gernal actions: Wind actions*. Eurocode 1. Brussels, Belgium: CEN.

Churchfield, M. J., G. Vijayakumar, J. G. Brasseur, and P. J. Moriaty. 2010. "Wind energy-related atmospheric boundary layer large-eddy simulation using OpenFOAM." In *19th Symp. on Boundary Layers and Turbulence*. Keystone, CO.

Counihan, J. 1975. "Adiabatic atmospheric boundary layers: A review and analysis of data from the period 1880–1972." *Atmos. Environ. (1967)* **9** (10): 871–905.

Davenport, A. G. 1968. "The dependence of wind loads on meteorological parameters." In *Proc., Int. Research Seminar on Wind Effects on Buildings and Structures*, 19–82. Toronto.

Drobinski, P., P. Carlotti, R. K. Newsom, R. M. Banta, R. C. Foster, and J.-L. Redelsperger. 2004. "The structure of the near-neutral atmospheric surface layer." *J. Atmos. Sci.* **61** (6): 699–714.

ESDU (Engineering Sciences Data Unit). 2001. *Characteristics of atmoshpheric turbulence near the ground. Part II: Single point data for strong winds (neutral atmosphere)*. ESDU 85020. ESDU.

Fichtl, G. H., and G. E. McVehil. 1970. "Longitudinal and lateral spectra of turbulence in the atmospheric boundary layer at the Kennedy Space Center." *J. Appl. Meteorol.* **9** (1): 51–63.

Grötzbach, G. 1987. "Direct numerical and large eddy simulation of turbulent channel flows." In *Encyclopaedia of fluid mechanics*, edited by N. P. Cheremisinoff, 6th ed., 1337–1391. Houston, TX: Gulf Publishing Company.

HE (Highways England). 2001. "Volume I: Highway structures: Approval procedures and general design." In *Design manual for roads and bridges (DMRB)*. HE.

Hémon, P., and F. Santi. 2007. "Simulation of a spatially correlated turbulent velocity field using biorthogonal decomposition." *J. Wind Eng. Ind. Aerodyn.* **95** (1): 21–29.

Hess, G. D. 2004. "The neutral, barotropic planetary boundary layer, capped by a low-level inversion." *Boundary Layer Meteorol.* **110** (3): 319–355.

Huang, S. H., Q. S. Li, and J. R. Wu. 2010. "A general inflow turbulence generator for large eddy simulation." *J. Wind Eng. Ind. Aerodyn.* **98** (10–11): 600–617.

Kaimal, J. C., J. C. Wyngaard, Y. Izumi, and O. R. Coté. 1972. "Spectral characteristics of surface-layer turbulence." *Q. J. R. Meteorol. Soc.* **98** (417): 563–589.

Kataoka, H., and M. Mizuno. 2002. "Numerical flow computation around aeroelastic 3D square cylinder using inflow turbulence." *Wind Struct.* **5** (2–4): 379–392.

Kondo, K., S. Murakami, and A. Mochida. 1997. "Generation of velocity fluctuations for inflow boundary condition of LES." *J. Wind Eng. Ind. Aerodyn.* **67–68**: 51–64.

Kozmar, H. 2011. "Wind-tunnel simulations of the suburban ABL and comparison with international standards." *Wind Struct.* **14** (1): 15–34.
Mason, P. J., and D. J. Thomson. 1992. "Stochastic backscatter in large-eddy simulations of boundary layers." *J. Fluid Mech.* **242**: 51–78.
Munters, W., C. Meneveau, and J. Meyers. 2016. "Turbulent inflow precursor method with time-varying direction for large-eddy simulations and applications to wind farms." *Boundary Layer Meteorol.* **159** (2): 305–328.
Nozawa, K., and T. Tamura. 2001. "Simulation of rough-wall turbulent boundary layer for LES inflow data." In *Proc., Second Int. Symp. on Turbulence and Shear Flow Phenomena*, 443–448.
OpenFOAM. 2015. *The open source CFD toolbox: User guide (version 2.4.0)*. OpenFOAM Foundation.
Park, S., and D. Yeo. 2016. *Database-assisted design and second-order effects on the wind-induced structural behavior of high-rise buildings*. Gaithersburg, MD: NIST.
Pasquill, F., and H. E. Butler. 1964. "A note on determining the scale of turbulence." *Q. J. R. Meteorol. Soc.* **90** (383): 79–84.
Porté-Agel, F., C. Meneveau, and M. B. Parlange. 2000. "A scale-dependent dynamic model for large-eddy simulation: Application to a neutral atmospheric boundary layer." *J. Fluid Mech.* **415**: 261–284.
Richards, P. J., and R. P. Hoxey. 1993. "Appropriate boundary conditions for computational wind engineering models using the k-[epsilon] turbulence model." *J. Wind Eng. Ind. Aerodyn.* **46–47**: 145–153.
Samali, B., K. C. S. Kwok, G. S. Wood, and J. N. Yang. 2004. "Wind tunnel tests for wind-excited benchmark building." *J. Eng. Mech.* **130** (4): 447–450.
Schumann, U. 1975. "Subgrid scale model for finite difference simulations of turbulent flows in plane channels and annuli." *J. Comput. Phys.* **18** (4): 376–404.
Shi, L., and D. Yeo. 2016. *OpenFOAM large-eddy simulations of atmospheric boundary layer turbulence for wind engineering applications: NIST Technical Note 1944*. Gaithersburg, MD: NIST.
Shi, L., and D. Yeo. 2017. "Large Eddy simulations of model-scale turbulent atmospheric boundary layer flows." *J. Eng. Mech.* **143** (9): 06017011.
Simiu, E. 2011. *Design of buildings for wind: A guide for ASCE 7-10 Standard users and designers of special structures*. Hoboken, NJ: Wiley.
Simiu, E., G. T. Bitsuamlak, A. G. Chowdhury, R. Li, A. Tecle, and D. Yeo. 2011. "Testing of residential homes under wind loads." *Nat. Hazard. Rev.* **12** (4): 166–170.
Simiu, E., and R. H. Scanlan. 1996. *Wind effects on structures*. Hoboken, NJ: Wiley.
Singer, I. A., N. E. Busch, and J. A. Frizzola. 1968. "The micrometeorology of the turbulent flow field in the atmospheric boundary surface layer." In *Int. Research Seminar on Wind Effects on Buildings and Structures*, 557–594. Ottawa.
Stull, R. B. 1988. *An introduction to boundary layer meteorology*. Dodrecht, Netherlands: Kluwer Academic Publishers.
Sutton, O. G. 1953. *Micrometeorology*. New York: McGraw-Hill.
Tabor, G. R., and M. H. Baba-Ahmadi. 2010. "Inlet conditions for large eddy simulation: A review." *Comput. Fluids* **39** (4): 553–567.
Tanaka, H., Y. Tamura, K. Ohtake, M. Nakai, Y. C. Kim, and E. K. Bandi. 2013. "Aerodynamic and flow characteristics of tall buildings with various unconventional configurations." *Int. J. High Rise Build.* **2** (3): 213–228.

Teunissen, H. W. 1970. *Characteristics of the mean wind and turbulence in the planetary boundary layer*. Institute for Aerospace Studies Review No. 32. Toronto: Univ. of Toronto.

Tominaga, Y. 2015. "Flow around a high-rise building using steady and unsteady RANS CFD: Effect of large-scale fluctuations on the velocity statistics." *J. Wind Eng. Ind. Aerodyn.* **142**: 93–103.

Vasaturo, R., I. Kalkman, B. Blocken, and P. J. V. van Wesemael. 2018. "Large eddy simulation of the neutral atmospheric boundary layer: Performance evaluation of three inflow methods for terrains with different roughness." *J. Wind Eng. Ind. Aerodyn.* **173**: 241–261.

Vickery, B. J. 1970. "On the reliability of gust loading factors." In *Proc., Technical Meeting Concerning Wind Loads on Buildings and Structures*. Washington, DC.

Wu, X. 2017. "Inflow turbulence generation methods." *Ann. Rev. Fluid Mech.* **49** (1): 23–49.

Xie, Z.-T., and I. P. Castro. 2008. "Efficient generation of inflow conditions for large eddy simulation of street-scale flows." *Flow Turbul. Combust.* **81** (3): 449–470.

Yang, X. I. A., G. I. Park, and P. Moin. 2017. "Log-layer mismatch and modeling of the fluctuating wall stress in wall-modeled large-eddy simulations." *Phys. Rev. Fluids* **2** (10): 104601.

Yeo, D., and A. Chowdhury. 2013. "Simplified wind flow model for the estimation of aerodynamic effects on small structures." *J. Eng. Mech.* **139** (3): 367–375.

Yoshizawa, A., and K. Horiuti. 1985. "A statistically-derived subgrid-scale kinetic energy model for the large-eddy simulation of turbulent flows." *J. Phys. Soc. Jpn.* **54** (8): 2834–2839.

Zilitinkevich, S. 2012. "The height of the atmospheric planetary boundary layer: State of the art and new development." In *National security and human health implications of climate change*, edited by H. J. S. Fernando, Z. Klaić, and J. L. McCulley, 147–161. Dordrecht, Netherlands: Springer.

Zilitinkevich, S., I. Esau, and A. Baklanov. 2007. "Further comments on the equilibrium height of neutral and stable planetary boundary layers." *Q. J. R. Meteorol. Soc.* **133** (622): 265–271.

Zilitinkevich, S. S., and I. N. Esau. 2002. "On integral measures of the neutral barotropic planetary boundary layer." *Boundary Layer Meteorol.* **104** (3): 371–379.